

## Roof plane extraction from airborne lidar point clouds

Rujun Cao, Yongjun Zhang, Xinyi Liu & Zongze Zhao

To cite this article: Rujun Cao, Yongjun Zhang, Xinyi Liu & Zongze Zhao (2017) Roof plane extraction from airborne lidar point clouds, International Journal of Remote Sensing, 38:12, 3684-3703, DOI: [10.1080/01431161.2017.1302112](https://doi.org/10.1080/01431161.2017.1302112)

To link to this article: <https://doi.org/10.1080/01431161.2017.1302112>



Published online: 24 Mar 2017.



[Submit your article to this journal](#)



Article views: 137



[View related articles](#)




[View Crossmark data](#)



Citing articles: 2 [View citing articles](#)



# Roof plane extraction from airborne lidar point clouds

Rujun Cao, Yongjun Zhang, Xinyi Liu  and Zongze Zhao

School of Remote Sensing and Information Engineering, Wuhan University, Wuhan, China

## ABSTRACT

Planar patches are important primitives for polyhedral building models. One of the key challenges for successful reconstruction of three-dimensional (3D) building models from airborne lidar point clouds is achieving high quality recognition and segmentation of the roof planar points. Unfortunately, the current automatic extraction processes for planar surfaces continue to suffer from limitations such as sensitivity to the selection of seed points and the lack of computational efficiency. In order to address these drawbacks, a new fully automatic segmentation method is proposed in this article, which is capable of the following: (1) processing a roof point dataset with an arbitrary shape; (2) robustly selecting the seed points in a parameter space with reduced dimensions; and (3) segmenting the planar patches in a sub-dataset with similar attributes when region growing in the object space. The detection of seed points in the parameter space was improved by mapping the accumulator array to a 1D space. The range for region growing in the object space was reduced by an attribute similarity measure that split the roof dataset into candidate and non-candidate subsets. The experimental results confirmed that the proposed approach can extract planar patches of building roofs robustly and efficiently.

## ARTICLE HISTORY

Received 25 September 2016

Accepted 17 February 2017

## 1. Introduction

Three-dimensional (3D) digital building models are necessary for 3D geographic information systems (GIS) and, therefore, play an important role in numerous applications for urban management. Since the data acquired by lidar systems are dense, accurate, georeferenced, as well as 3D (Leberl et al. 2010; Toth and Józków 2016), they are the natural choice for reconstructing building models (Haala and Kada 2010; Rottensteiner et al. 2014). Polyhedron buildings are quite common in urban areas (Sampath and Shan 2010). As a result, polyhedral models that represent buildings as rather simple planar patches are sufficient for various applications. Furthermore, they can be reconstructed in a fully automatic manner with specific levels of detail (Kwak and Habib 2014; Meidow and Hammer 2016; Sun 2013; Xiong et al. 2015; Zhou 2012).

Building reconstruction from airborne lidar data is principally based on the segmentation of the raw data sets into building points or building regions. Building footprints

extraction from lidar point clouds commonly involves two successive steps, i.e. filtering and segmentation. There are dozens of established filtering algorithms available such as morphological filter (Chen et al. 2013; Pingel, Clarke, and McBride 2013; Zhang et al. 2003), progressive triangular irregular network (TIN) densification filter (Axelsson 2000), and multi-directional ground filtering (Meng et al. 2009). To extract only building points, non-ground points are further classified based on shape measures or roughness of the point clouds. Density based segmentation (Filin and Pfeifer 2006),  $k$ -plane clustering ( $k$  is the desired number of clusters) (Kong et al. 2014; Kong, Xu, and Li 2013), region growing (Rabbani, Van Den Heuvel, and Vosselman 2006; Zhang, Yan, and Chen 2006) or eigenvalue analysis of local covariance matrix (Awrangjeb and Fraser 2014; Sampath and Shan 2010; Verma, Kumar, and Hsu 2006) can be used for this purpose. In the work of Xu, Kong and Li (2014), the input scan lines were rasterized and analysed with wavelet transform to extract polyhedral buildings in real time. Sun and Salvaggio (2013) first removed vegetations by a graph cuts based method and then extracted buildings based on a hierarchical Euclidean clustering.

To reconstruct a 3D building model with high accuracy and precision from airborne lidar point clouds, the first step is to recognize and segment the roof planar patches at a higher level of quality, since they serve as important primitives (Kim et al. 2016; Nurunnabi, Belton, and West 2014; Sampath and Shan 2010). The task for planar region segmentation is to cluster points that belong to the same plane based on their similarity and proximity. Generally, there are two groups of techniques to segment planar features from raw lidar data: (1) segmentation in object (spatial) space and (2) segmentation in parameter (attribute) space (Kim et al. 2016; Vosselman and Gorte 2004).

Region growing with a seed point is one of the most common spatial domain methods utilized to detect roof planar facets (Lari and Habib 2014; Rabbani, Van Den Heuvel, and Vosselman 2006; Sun 2013; Sun and Salvaggio 2013; Vosselman and Gorte 2004); however, this method is sensitive to the selection of seed points and not sufficiently robust (Wang and Shan 2009). Random sample consensus (RANSAC) (Fischler and Bolles 1981) is a generally robust but computation-complicated approach to estimate planar parameters by randomly sampling data points in the object space and enlarging the set with as consistent data as possible (Verma, Kumar, and Hsu 2006). In contrast to the segmentation process in spatial domain approaches, the selection of seed points is not necessary in segmenting planar patches in a parameter domain; but the result depends heavily on the estimated attributes that are usually computed within a local neighbourhood. The most common attributes are normal vectors, which are derived for a particular point from different neighbourhoods (Axelsson 1999; Filin and Pfeifer 2006; Kim et al. 2016; Kong et al. 2014; Lari and Habib 2014; Vosselman and Gorte 2004). When estimating the attributes for each lidar point, the classical Hough transformation (Ballard 1981; Duda and Hart 1972) is extended to detect planes (Vosselman and Dijkman 2001). However, segmentation in the parameter domain still lacks the computational efficiency necessary for a large scale of points.

To address this problem, this article proposes a segmentation approach that (1) processes roof point datasets with concave shapes as well as convex shapes; (2) maps the plane normals from the 3D parameter space to a 1D space and robustly selects the seed points in the parameter space with reduced dimensions; and (3) segments the planar patches in a sub-dataset with similar attributes during the growing process in

object space when the region growing is limited within the subset to achieve efficiency. Furthermore, the proposed method works in a fully automatic manner.

## 2. Methodology

This section introduces a hybrid method, which extracts planar patches from airborne lidar points by automatically selecting seed points in a parameter domain and then growing them in a spatial domain. The primary steps include: (1) the selection of attributes and their computation, (2) clustering in a parameter space to select the seed points, (3) region growing in the spatial space to segment the planar patches, and (4) fitting the planar equations using the least squares fit (LSF) method. [Figure 1](#) depicts the principal steps for the proposed planar patch extraction approach.

The lidar datasets used in this study are classified as ‘building’ regions (Zhao et al. 2016). The modified convex hull boundary detection algorithm, which limits candidates in a local rectangular neighbourhood (Jarvis 1977; Moreira and Santos 2007; Sampath and Shan 2007) is utilized to determine the initial boundary of individual buildings. After tracing the approximate boundary, Delaunay triangulation with boundary constraints is presented, and the normalized vector of each triangle is computed and quantified in the parameter space. The histogram for normal vectors is accumulated to detect local peaks

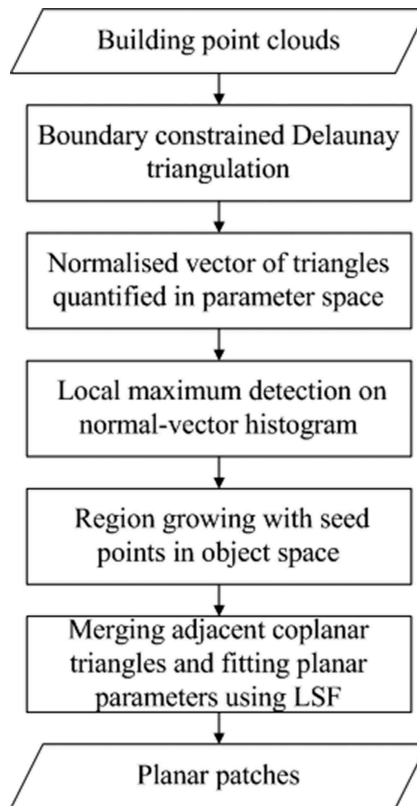


**Figure 1.** Flow chart for building planar patch extraction.

and each peak represents similar attributes, i.e. parallel or coplanar planes. Starting from a triangle with these attributes, spatial connectivity analysis is performed in the object space, iteratively grown to obtain an initial roof plane, and coplanar or parallel planes are separated. Finally, the triangles labelled as the same group are merged to form a polygon and the vertices associated with the triangles that are located on the same plane are fitted by the LSF method to compute the parameters for the planar equation. The following subsections illustrate these procedures in more detail.

## 2.1 Selection for planar attributes

In mathematics, a plane is a flat, 2D surface that infinitely extends with zero thickness. Given three points that are not collinear in a 3D space, there is just one plane that contains all the three. In 3D Euclidean space  $\mathbb{R}^3$ , planes have a natural description using a point in the plane and a vector orthogonal to it (normal vector) to indicate its 'inclination':

$$\mathbf{n} \cdot (\mathbf{r} - \mathbf{r}_0) = 0. \quad (1)$$

Equation (1) is the equation of a plane in the point-normal form, where the dot means dot product,  $\mathbf{n}$  is the normal vector (non-zero),  $\mathbf{r}$  is the position vector (an arbitrary point in the plane), and  $\mathbf{r}_0$  is a given point in the plane. When representing a vector in the standard basis of the 3D Euclidean space, the general form of the equation of a plane is as follows:

$$ax + by + cz + d = 0, \quad (2)$$

where  $\mathbf{n} = (a, b, c)$  is the normal vector and  $d = -\mathbf{n} \cdot \mathbf{r}_0 = -(a x_0 + b y_0 + c z_0)$  is related to the distance from the origin.

If there are three non-collinear points,  $P_0(x_0, y_0, z_0)$ ,  $P_1(x_1, y_1, z_1)$ , and  $P_2(x_2, y_2, z_2)$ , the equation can be derived as

$$\mathbf{n} \cdot (\mathbf{r} - \mathbf{p}) = 0, \quad (3)$$

where  $\mathbf{n} = (P_1 - P_0) \times (P_2 - P_0)$ , i.e. the normal vector is the cross product of the two vectors, and  $\mathbf{p}$  is a vector of any of the given points  $P_0$ ,  $P_1$ , or  $P_2$ . The normal vector  $\mathbf{n}$  can be normalized as a unit normal vector  $\hat{n}(n_x, n_y, n_z)$ , using Equation (4):

$$n_x = \frac{a}{\sqrt{a^2 + b^2 + c^2}}, n_y = \frac{b}{\sqrt{a^2 + b^2 + c^2}}, n_z = \frac{c}{\sqrt{a^2 + b^2 + c^2}}. \quad (4)$$

It is obvious that a plane has two attributes, i.e. position (position vector) and inclination (normal vector). However, planar patches are finite surfaces which are confined within their boundaries. The fact that multiple patches may have exactly the same attributes (co-planar) requires differentiating them from their spatial connectivity.

For a given unstructured point set, Delaunay triangulation forms a triangular mesh of its convex hull (De Berg et al. 2008). When the unstructured lidar point dataset is structured via Delaunay triangulation, the neighbourhood of each point is determined. Since the boundary of a building is not always 'convex', triangulating the building points with constraints is desired (Du and Wang 2004; Shewchuk 2002). The tracing of building boundaries is beyond this article and readers may refer to (Awrangjeb 2016;

Edelsbrunner, Kirkpatrick, and Seidel 1983; Graham 1972; Jarvis 1977; Moreira and Santos 2007; Sampath and Shan 2007) for more details on that topic.

Each triangle of the triangulation of the lidar building points determines a plane equation which can be easily derived using Equation (3) and triangles located on the same plane have similar properties. To estimate the normal of a point, a prerequisite is the finding for the neighbours of the point. Distance measures, or spatial relationships determine the neighbourhood of a point. For example, a physical distance in  $\square^2$  defines a circular (Euclidean distance) or rectangular (Manhattan or Chebyshev distance) neighbourhood; and similarly for the  $k$ -nearest or Voronoi neighbours. However, the determination of a proper value for the threshold (distance threshold, or  $k$ ) requires domain knowledge. Furthermore, due to noises or range errors, the desired normal of some points may have bias (Kong, Xu, and Li 2013). In contrast to the point normal that is derived from a fitted surface within its neighbourhoods, the normal vector of a triangle is more intuitive and more feasibly obtained. Hence, we select the normalized vector of a triangle as the planar patches' parameter to cluster them in an attribute domain. The normal of each triangle is calculated and normalized after the boundary-constrained triangulation process.

## 2.2 Selection of seed points

Since raw lidar point clouds are not noise-free and building roofs have rough surfaces, the normal of a single triangle is not robust enough for the selection process. To obtain robust results, the seed points for planar patches must be selected with statistical significance. When mapped onto a Gauss Sphere (hemisphere), the unit vectors of the coplanar (or parallel) triangles point the same direction, and the saliencies are formed on the sphere (Figures 2(a–c)). Therefore, when the normal vector of each triangle was computed in this article after Delaunay triangulation with boundary constraints, a histogram for the attributes of the normals was used to detect peaks. These saliencies

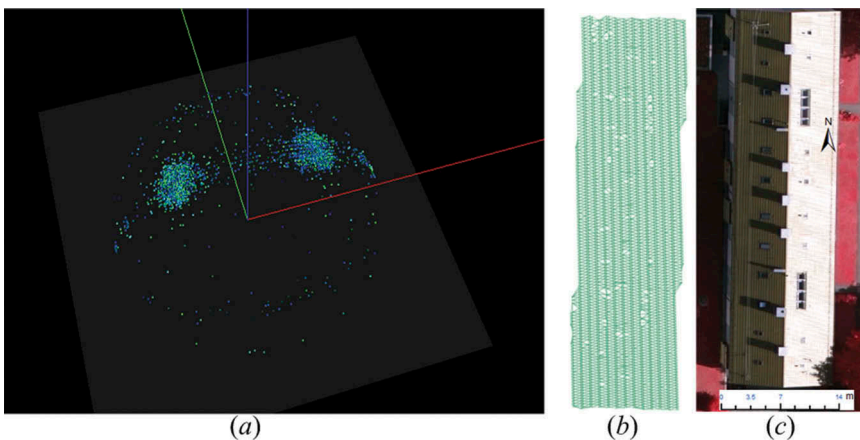


**Figure 2.** Unit normals of triangles (for a gable roof) mapped onto a Gauss Sphere (a); (b) triangulated lidar points; and (c) reference image.

on the Gaussian sphere or the local maxima on the histogram defined the most likely direction of roof planar segments.

Similar to the voting scheme used in Hough Transform, an accumulator array is introduced to construct the histogram for the normal vectors. The dimension of the accumulator array is determined by the number of parameters. For a normalized vector of a plane in  $\mathbb{R}^3$ , the three components have only two free variables. Although a 2D accumulator can be used in the voting, we deliberately left it as a 3D configuration space (corresponding to the three components of the vector,  $n_x$ ,  $n_y$ , and  $n_z$ ) for clarity and computation efficiency. The configuration space forms a cube in which each component has a continuous range of  $[-1, 1]$ ; but for triangles in the triangulation from airborne lidar points, it is reasonable to limit the  $n_z$  component within the range of  $[0, 1]$ .

To construct the histogram of the unit vectors, each component of the vector needs to be quantified as a discrete value. The step size (or bin cell size) needs to be balanced between the accuracy and reliability necessary for plane detection. The smaller the step size, the more accurate the parameter values will be for the plane to be extracted; and since they are more susceptible to the noise, the size of the accumulator array also will be larger. However, the array of a 3D histogram is memory-expensive, especially for a small-sized bin. A possible solution to this problem is to split the 3D parameter space into 2D sub-spaces with a higher computation complexity. Fortunately, when noticing that many cells of the array are mapped to a null value, the 3D array is mapped to a 1D array, using a tuple  $(i, j, k, \text{value})$  representing a cell, where  $i, j$ , and  $k$  can be mapped to a 1D index (Figure 3). This representation is inefficient if the array is dense. Therefore, the algorithm adapts to the array length of the histogram and the number of normal vectors (triangles). In other words, when the ratio between the number of triangles and the array size exceeds a threshold (0.8 in this article), it does not apply the mapped mode, i.e. the dimension of the accumulator array is not reduced and remains at three.

### 2.3 Planar patch segmentation in spatial space

Considering the accuracy of data acquisition, the selection for quantization of the interval (step size) and computation errors, 'attribute similarity' is defined by a Chebyshev distance (Minkowski infinity-norm distance), which is related to the step size.

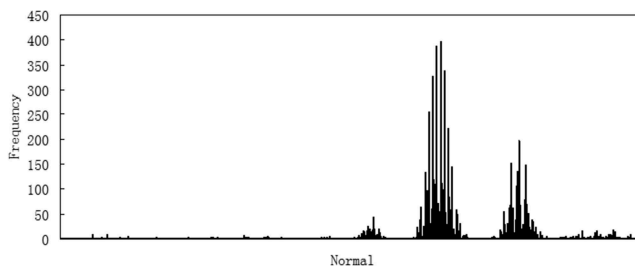


**Figure 3.** Linearized 3D normal histogram (for a gable roof).

**Definition 1:**  $a$  Resembles  $b \Leftrightarrow \text{Distance}(a, b) \leq d_{\text{threshold}} \Leftrightarrow \max(|a - b|) \leq d_{\text{threshold}}$ .

For a given point  $p$  in the normal histogram, its ‘neighbours’ are similar to  $p$  if their distance to  $p$  is less than or equal to a pre-determined threshold  $d_{\text{threshold}}$  in the 3D attribute space. For example, if  $d_{\text{threshold}} = 1$ , point  $p$  and its 26 neighbours ( $b$ ) form a  $3 \times 3 \times 3$  cube, i.e.  $\max(|p_x - b_x|, |p_y - b_y|, |p_z - b_z|) \leq d_{\text{threshold}} = 1$ .

The triangle set  $S$  is split into two subsets according to its normal components: candidate subset  $S_1$ , which has similar attributes with a local peak in the histogram, and non-candidate  $S_2$  for the others. The growing for the surface, which is based on spatial proximity, is restricted in the candidate subset  $S_1$ , but not the universal set  $S$ . The definition of the adjacency of a triangle is as Definition 2, i.e. the two adjacent triangles share at least one common vertex, but do not overlap:

**Definition 2:**  $a$  Adjoins  $b \Leftrightarrow ((a \cap b \neq \emptyset) \wedge \text{Area}(a \cap b) = 0)$ .

After the construction of the normal histogram, region growing begins from a triangle whose attributes are similar to a local peak in the histogram. Every local peak represents the similar attributes for the planar normal vectors in the parameter space (parallel or coplanar in spatial space); thus, spatial connectivity analysis is applied to separate these coplanar or parallel patches. The segmentation procedure in this article is as follows and as shown in [Figure 4](#):

- (1) select an unvisited local peak from the histogram and construct the subset  $S_1$ , in which every member has a similar attribute to the peak;
- (2) select an arbitrary member from  $S_1$  (the seed point);
- (3) add the seed point to a candidate set  $C$  and remove it from  $S_1$  (labelling);
- (4) for each member in  $C$ , find and add all its adjacencies into  $C$  from  $S_1$  until there are no adjacencies in  $S_1$  (region growing);
- (5) repeat steps (2), (3), and (4) until  $S_1$  is empty (another patch); and
- (6) mark the local peak as visited and repeat the former steps if there are any other peaks.

## 2.4 Computation for plane equation

After the triangles labelled as the same group are merged to form a polygon in 3D space, the vertices associated with these triangles located on the same plane are fitted by a LSF method to compute the parameters of the plane equation. As roof planes generally are not vertical, each one can be described by the equation:

$$z = ax + by + d. \quad (5)$$

Additionally, to avoid solving an ill-conditioned system of linear equations when using LSF, another form of planar equation is also commonly used (Equation (6)):

$$z - \bar{z} = a(x - \bar{x}) + b(y - \bar{y}), \quad (6)$$

where  $\bar{x}$ ,  $\bar{y}$ , and  $\bar{z}$  denote the mean of  $\sum x_i$ ,  $\sum y_i$ , and  $\sum z_i$ , respectively.



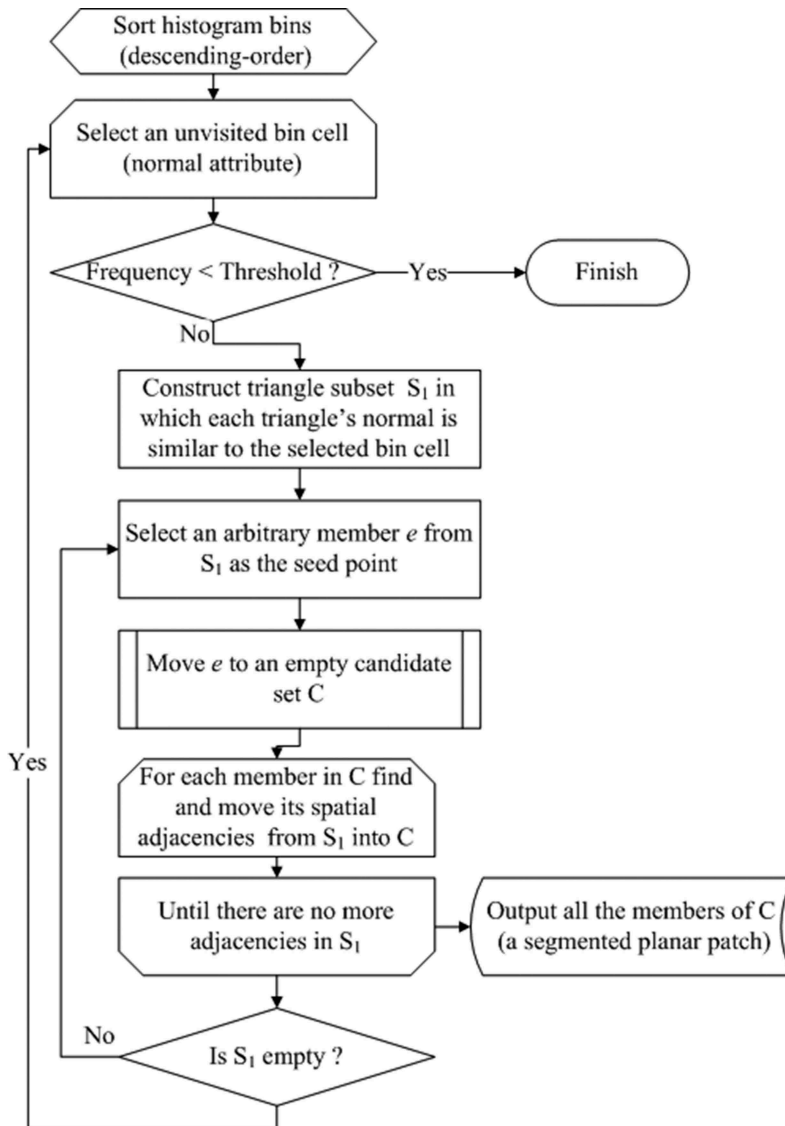


**Figure 4.** Flow chart for planar patch segmentation in spatial space.

While a plane equation is fitted using Equation (5) or Equation (6), the errors are measured vertically. Alternatively, the errors can be measured orthogonally to the proposed plane using Equation (1). It can be found by standard eigen system solvers using orthogonal regression, and the corresponding unit length eigenvector completes the construction of the least squares plane. In this article, Equation (5) is applied to fit the parameters of a plane because of its computational efficiency and there are sufficient samples and outliers rarely occur during the clustering process.

Some factors, such as the nature of the lidar data acquisition and the roughness of the roof surfaces, quantization, and/or computation errors may result in that the originally coplanar triangles have dissimilar attributes and are excluded during the

clustering process. Therefore, those coplanar triangles are to be included during the planar patch extraction process by verifying the co-planarity conditions. This problem is discussed in the following two cases:

The first case is when some of the triangles are not grouped with their neighbours because their attributes are inconsistent with their adjacencies. These triangles result in holes or gaps in the plane, but their three vertices are all in the planar patch. In this case, if a triangle's two or three 'sided' adjacent triangles have the same properties, its attributes are updated to that of their neighbours and merged with them (Figure 5).

The second case occurs when some other triangles are not clustered after the clustering process. In this situation, one of these triangles is verified with the two coplanar conditions, i.e. (1) the intersection angle with its adjacent planar patch and (2) the vertex residuals on the plane. If all conditions are satisfied (values less than the thresholds), the triangle is merged into its neighbouring planar patch.

### 3. Experiments and discussion

To analyse the performance of the proposed method, several experiments were carried out, which are discussed in Section 3.1 along with the quantitative evaluations. The threshold selection process is discussed in Section 3.2.

#### 3.1 Experiments

The Vaihingen dataset was selected to test the proposed method. The airborne lidar point cloud was acquired using a Leica ALS50 laser scanning system. Its accuracy is about 10 cm in planarity and vertical and the average point density varies from 4 to 6.7 points  $m^{-2}$  (Rottensteiner et al. 2014). Our method is based on PostGIS, which extends PostgreSQL with robust spatial database management capabilities.

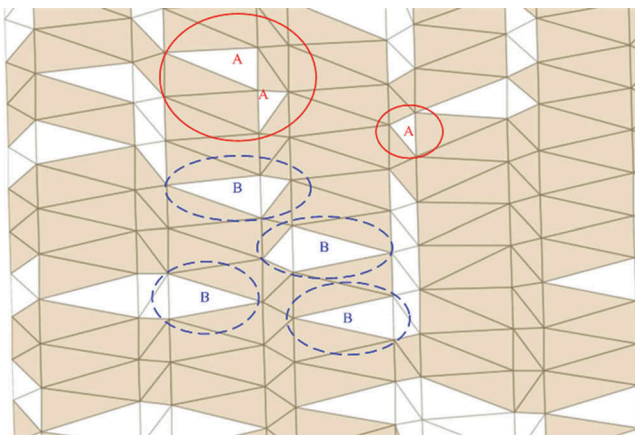


**Figure 5.** Missed triangles during clustering process: the normal components of the red-circled (marked as A) triangles differ from their three neighbours, while the blue-dashed circles (labelled as B) differ from the twos; but all the three vertices of these triangles are co-planar with their neighbours. Thus, these triangles are segmented in the same group with their vicinities.

For each component of the normalized vector  $\mathbf{v}$ , we quantified the continuous space by an interval of 0.05, i.e. the histogram had 40, 40, and 20 bins for the  $v_x$ ,  $v_y$  and  $v_z$  components, respectively. Thus, the histogram array had  $40 \times 40 \times 20 = 32,000$  bin cells. Since a patch that can be robustly detected has a minimum number of points, a local peak in the normal histogram has a minimum frequency of 4 in this article (four triangles, if they are compact adjacent, share five vertices). The angle threshold value of  $12^\circ$  was used in these experiments, which is related to the vertical accuracy and the average point spacing of the dataset (Section 3.2).

Figures 6(a–f) illustrate the planar patch extraction process for a gable roof (Building 1). The raw dataset had 3290 points. There were 6332 triangles after the boundary-constrained triangulation while the linearized normal histogram had 455 bins for all the normals (Figure 3). The distribution of the normal is presented in Figures 2(a–c). Three planar patches were extracted with an area greater than  $3.00 \text{ m}^2$ , including a patch near the ridge that had an area of  $3.04 \text{ m}^2$  (Figure 6(e), circled in red). Some evaluations for the extracted planar patches are indicated in Table 1. Please note that the points lying in various patches (shared boundary points) were calculated repetitively.

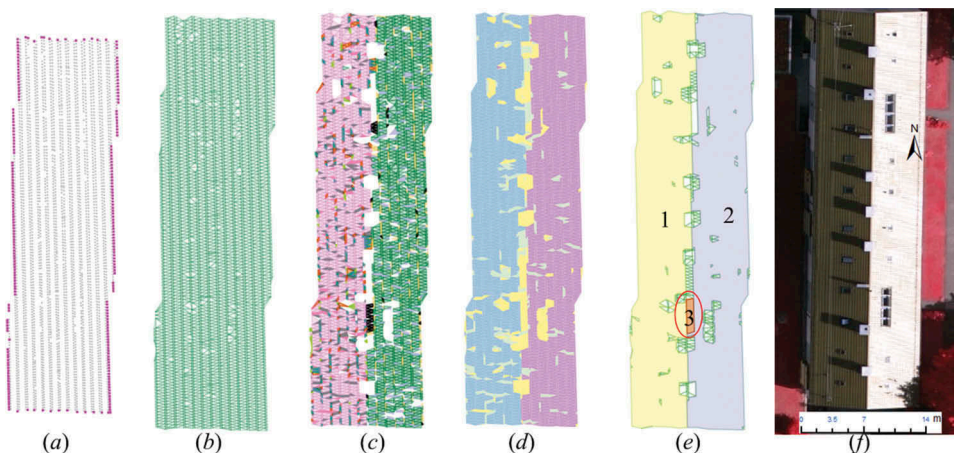


**Figure 6.** Planar patch segmentation process for a gable roof (Building 1): (a) raw lidar points with traced boundary (purple dots), (b) Delaunay triangulation with boundary constraint, (c) distribution of the triangle's normal vector (the same value mapped to the same colour), (d) clustering result for region growing with seed points within a similar triangle subset, (e) planar patch extraction result after merging the missed coplanar triangles, and (f) reference image.

**Table 1.** Evaluations for the extracted planar patches of Building 1.

Patch no.	Area ( $\text{m}^2$ )	Grouped points	Max-residual (vertical) (m)	RMSE (m) (vertical)	Max-residual (orthogonal) (m)	RMSE (m) (orthogonal)
1	260.60	1604	0.23	0.02	0.20	0.02
2	268.54	1649	0.21	0.03	0.19	0.02
3	3.04	24	0.06	0.03	0.06	0.03

'Area' is the projected area on a horizontal plane; 'Max-residual' indicates the maximum absolute value of the residual error in meters (m); and 'RMSE' indicates root mean square error.

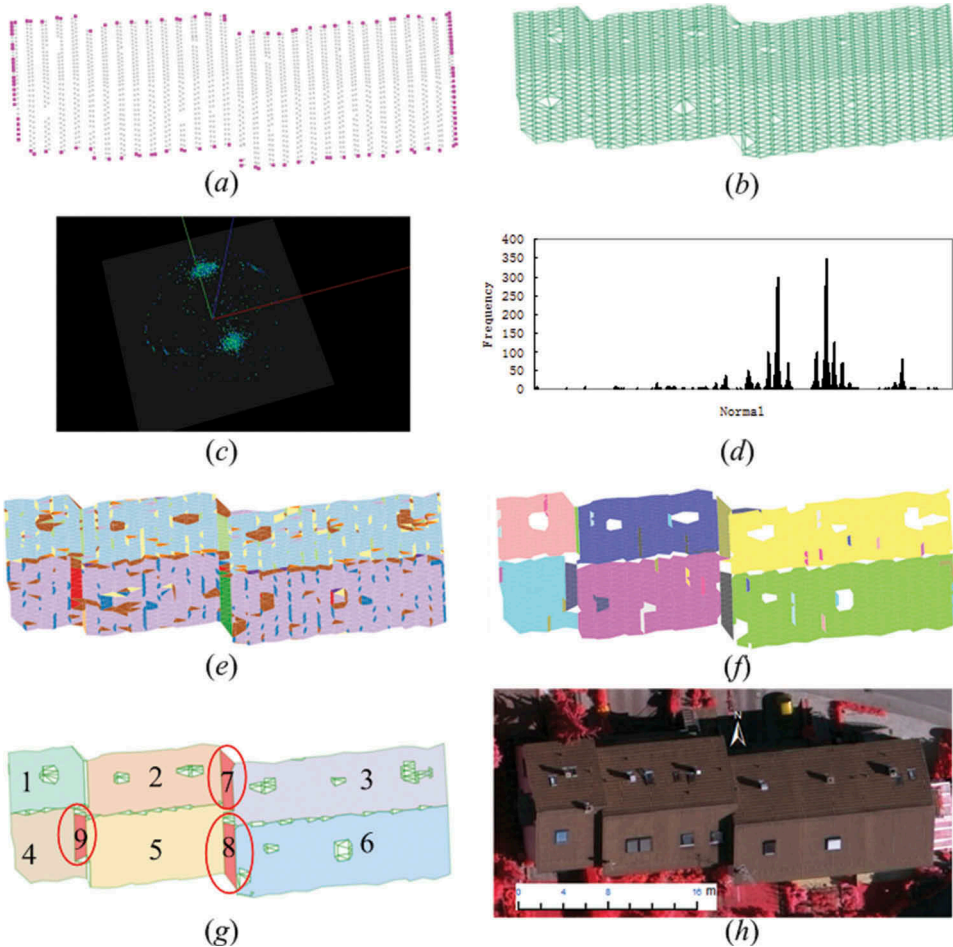


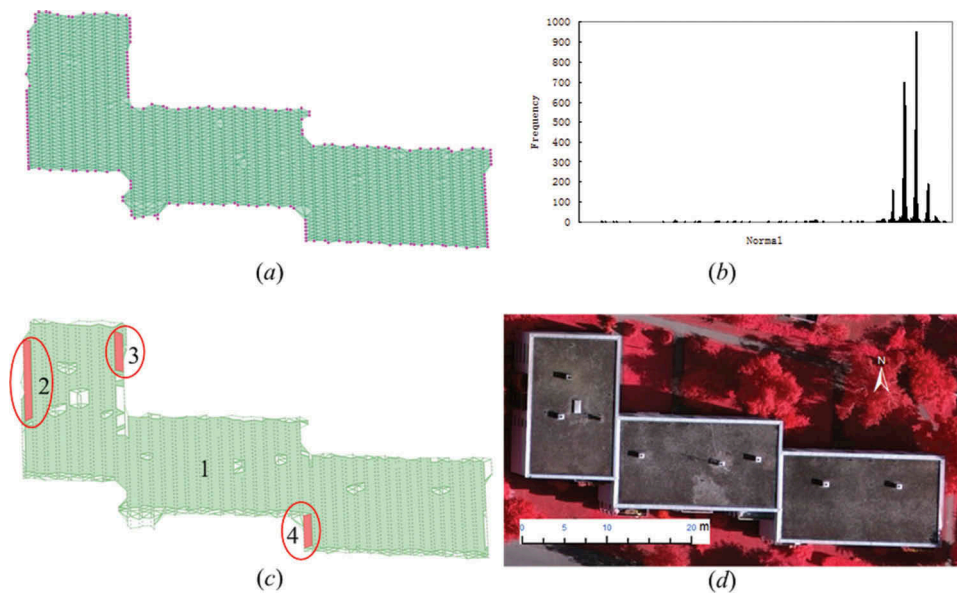
**Figure 7.** Planar patch extraction for a multiple-gable roof (Building 2): (a) raw points with traced boundary (purple dots), (b) Delaunay triangulation with the boundary constraint, (c) distribution of the normalized vectors, (d) histogram of the normals, (e) triangles grouped with a similar normal attribute, (f) planar patches clustered in spatial space (parallel patches are segmented via connectivity analysis), (g) planar patch extraction result (merging missed coplanar triangles), and (h) reference image.

The segmentation of the planar patches for a multiple-gable roof (Building 2) is presented in Figures 7(a–h). As can be seen from the distribution of its normalized vectors (Figure 7(c), two saliencies), or from the histogram (Figure 7(d), two significant peaks), there are two groups of parallel patches (Figure 7(e), same colour for each group). When clustering with seed points in spatial space, these patches were disjointed regions and were segmented by a spatial connectivity criterion (Figure 7(f)). In Figure 7(g), the patches circled in red that connect the two neighbouring parallel patches were vertical planes and needed to be improved (Table 2).

A dataset of flat roof points (Building 3) was used to test the proposed method in this article (Figures 8(a–d)). The roof was characterized by flat patches enclosed with parapet walls (Figure 8(d)). Because the points sampled by the laser scanning system hardly

**Table 2.** Evaluations for the extracted planar patches of Building 2.

Patch no.	Area (m <sup>2</sup> )	Grouped points	Max-residual (vertical) (m)	RMSE (m) (vertical)	Max-residual (orthogonal) (m)	RMSE (m) (orthogonal)
1	30.81	176	0.09	0.02	0.08	0.02
2	57.11	318	0.18	0.03	0.16	0.02
3	91.89	540	0.10	0.02	0.09	0.02
4	32.62	134	0.06	0.02	0.05	0.02
5	72.35	290	0.20	0.03	0.18	0.03
6	107.10	463	0.13	0.02	0.11	0.02
7	4.45	29	0.21	0.07	0.15	0.05
8	4.87	23	0.08	0.02	0.04	0.01
9	3.70	19	0.08	0.03	0.06	0.02

**Figure 8.** Planar patch segmentation for a flat roof (Building 3): (a) boundary-constrained Delaunay triangulation (boundary points are purple dots), (b) histogram of normalized vectors, (c) planar patch extraction result (with raw lidar points dotted), and (d) reference image.**Table 3.** Evaluations for the extracted planar patches of Building 3.

Patch no.	Area (m <sup>2</sup> )	Grouped points	Max-residual (vertical) (m)	RMSE (m) (vertical)	Max-residual (orthogonal) (m)	RMSE (m) (orthogonal)
1	555.68	2334	0.23	0.03	0.23	0.03
2	7.63	43	0.07	0.02	0.05	0.02
3	4.00	22	0.04	0.01	0.04	0.01
4	3.26	18	0.15	0.04	0.14	0.04

covered the line features, these flat patches connected them to each other in spatial space. Meanwhile, some wall points and flat roof points formed inclined planes (Figure 8 (c)), and these 'false' patches needed to be improved during the reconstruction process. Quantitative evaluation of the extraction results is presented in Table 3.



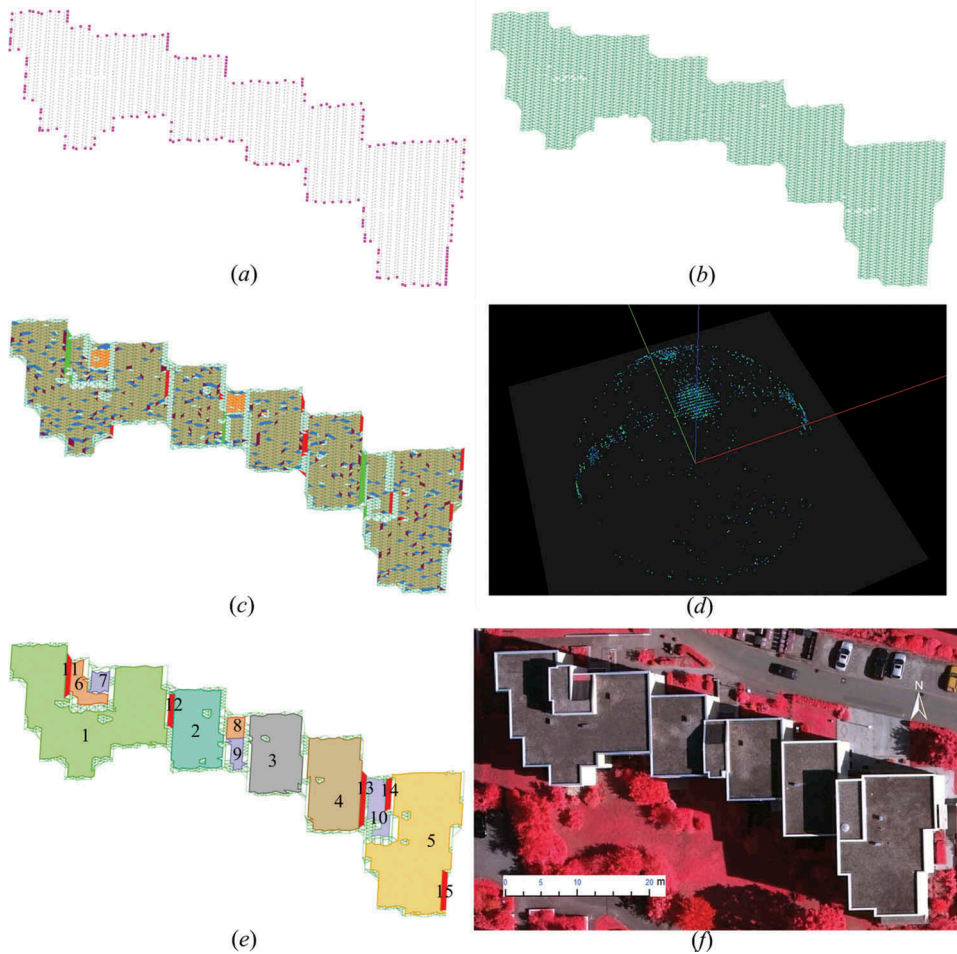


**Figure 9.** Planar patch extraction for a flat roof (Building 4): (a) raw lidar points with traced building boundary (purple dots), (b) boundary-constrained Delaunay triangulation, (c) triangles grouped with a similar normal attribute, (d) distribution of the normalized vectors on a Gauss sphere, (e) planar patch extraction result, and (f) reference image.

The proposed planar patch extraction method was also tested using another point set of a building with a flat roof (Building 4) (Figures 9(a–f)). The building had several roof patches close to horizontal. As can be seen from the distribution of the normalized vectors (Figure 9(d)), saliency around the z-axis (blue line) implied the similar normal attributes these patches shared. These ‘similar’ patches were separated during the process of region growing in spatial space. Quantitative evaluations of the extracted patches are presented in Table 4.

Figures 10(a–f) show the planar patch extraction process for a complex building roof (Building 5). The building had two intersecting gables, a connected gable, a shed roof, and a flat attachment (Figure 10(f)). Parallel patches (Figure 10(b), brown coloured) were spatially disjointed and thus were segmented into different patches via spatial proximity (Figure 10(c), labelled as 5 and 7). The flat patch (Figure 10(c), circled in blue-dashes) was

**Table 4.** Evaluations for the extracted planar patches of Building 4.

Patch no.	Area (m <sup>2</sup> )	Grouped points	Max-residual (vertical) (m)	RMSE (m) (vertical)	Max-residual (orthogonal) (m)	RMSE (m) (orthogonal)
1	218.12	897	0.13	0.02	0.13	0.02
2	72.30	318	0.10	0.02	0.10	0.02
3	77.71	325	0.13	0.02	0.13	0.02
4	93.13	399	0.15	0.02	0.15	0.02
5	180.02	751	0.11	0.02	0.11	0.02
6	15.58	81	0.14	0.03	0.14	0.03
7	7.02	39	0.10	0.03	0.09	0.03
8	7.17	40	0.06	0.03	0.05	0.02
9	7.49	45	0.14	0.03	0.14	0.03
10	18.96	97	0.09	0.02	0.09	0.02
11	4.14	27	0.27	0.08	0.06	0.02
12	3.75	23	0.25	0.07	0.10	0.03
13	5.55	36	0.23	0.10	0.04	0.02
14	3.48	22	0.05	0.02	0.05	0.02
15	4.42	27	0.11	0.03	0.09	0.02

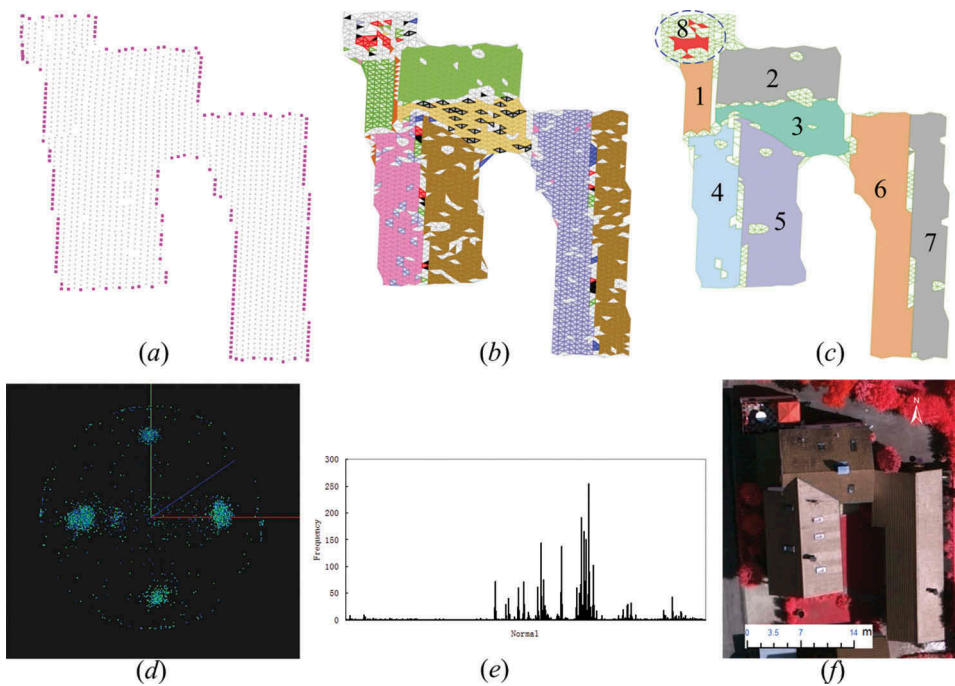


**Figure 10.** Planar patch extraction for a complex building roof (Building 5): (a) raw lidar points with traced building boundary (purple dots), (b) triangles grouped with similar attributes, (c) planar patch extraction results, (d) distribution of normalized vectors on a Gauss sphere, (e) histogram of normalized vectors, and (f) reference image.

extracted imprecisely due to the roof attachments and roof roughness. The planar patch extraction results are evaluated in Table 5.

The planar patch extraction results for the five buildings are summarized in Table 6. The maximum size of the histogram array (linearized) had a value of 646 (Building 4), which was about 2% of the length of the full array (32,000 cells). The proposed method

**Table 5.** Evaluations for the extracted planar patches of Building 5.

Patch no.	Area (m <sup>2</sup> )	Grouped points	Max-residual (vertical) (m)	RMSE (m) (vertical)	Max-residual (orthogonal) (m)	RMSE (m) (orthogonal)
1	17.50	81	0.06	0.02	0.06	0.02
2	55.61	225	0.17	0.02	0.13	0.02
3	40.46	185	0.16	0.03	0.13	0.02
4	58.15	257	0.16	0.03	0.13	0.02
5	76.70	309	0.16	0.03	0.14	0.03
6	97.45	446	0.15	0.03	0.13	0.02
7	73.91	344	0.15	0.03	0.13	0.03
8	4.76	32	0.08	0.03	0.08	0.03

**Table 6.** Summary of the extraction results for building roof planar patches.

Building no.	Number of points	Number of triangles	Accumulator array length	Ratio btw full array length (%)	Extracted patches ( $\geq 3$ m <sup>2</sup> )	Inaccurate patches	Reason for inaccuracy
1	3290	6332	455	1.42	3	1	Crossing ridge
2	1905	3674	350	1.09	9	3	Step-edge
3	2616	5018	398	1.24	4	3	Parapet-wall
4	3374	6457	646	2.02	15	5	Step-edge
5	1920	3609	467	1.46	8	1	Roof attachments

**Table 7.** Performance evaluation for the proposed planar extraction method.

Building no.	Number of triangles	Runtime for TIN (s)	Planar clustering (s)	Constrained clustering (s)	Improvements (%)	Improvement in total (%)
1	6332	2.294	8.907	7.567	17.7	13.6
2	3674	1.232	5.195	4.286	21.2	16.5
3	5018	1.966	7.675	7.226	6.2	4.9
4	6457	2.761	10.016	9.341	7.2	5.6
5	3609	1.420	5.288	4.132	28.0	20.8
Total	250,90	9.673	37.081	32.552	13.9	10.7

'Constrained clustering' indicates region growing with constraints of the attribute similarity; total runtime = TIN + clustering. All the tests run on the same platform, a Lenovo® T4900d-00 PC with 4 GB RAM, Intel® Core(TM)-i7-3770 CPU @3.4 GHz, ATA ST1000DM003 disk, Windows7 64-bit, PostgreSQL 9.4, and PostGIS 2.2.

significantly increased the efficiency of the process. There were also some extracted patches that needed to be improved during the reconstruction process, which were mainly affected by the break-lines (step-edges), parapet walls, or roof attachments and small areas.

We also evaluated the performance of the proposed method (Table 7) and compared it with a point-normal based planar segmentation method (PNS) (Sampath and Shan 2010). As shown in Table 7, the average runtime for the process of region growing with constraints of attribute similarity was about 13.9% less than the process without constraints, and the overall performance improvement was about 10.7%. As the most triangles of the two buildings (Building 3 and 4, flat-roofed) had similar normals, the improvements were not remarkable. Compared with the PNS method (Table 8), which took more time on the computation of the point normals within the Voronoi neighbourhoods of particular points, the runtime performance of the proposed method outperformed 24%.



**Table 8.** Comparison with a point-normal based method.

Building no.	Number of points	Point normal (s)	Clustering (s)	Total runtime (s)	This article (s)	Improvements (%)
1	3290	8.783	5.210	13.993	9.861	41.9
2	1905	3.854	2.808	6.662	5.518	20.7
3	2616	6.505	4.103	10.608	9.192	15.4
4	3374	9.703	4.649	14.352	12.102	18.6
5	1920	4.150	2.730	6.880	5.552	23.9
Total	13105	32.995	19.500	52.495	42.230	24.3

Total runtime' includes the time of the calculation for point normals and the time for grouping points with similarity and proximity. All the tests run on the same platform, a Lenovo® T4900d-00 PC with 4 GB RAM, Intel® Core(TM)-i7-3770 CPU @3.4 GHz, ATA ST1000DM003 disk, Windows7 64-bit, PostgreSQL 9.4, and PostGIS 2.2.

### 3.2 Discussion

The thresholds used in this article, such as the cell size of the histogram, the co-planarity conditions, and the selection process affected the results in specific ways; therefore, the threshold setting process is discussed in this section.

To compute the histogram of normal vectors, the components of the vector were discretized in attribute space. The parameter space of the 3D unit vector  $(v_x, v_y, v_z)^T$  formed a cube and each component had a continuous range of  $[-1, 1]$ . However, if the surface (normal) points 'up' was limited, the  $v_z$  component also was limited within the range of  $[0, 1]$  and the space shrank to half-size. As mentioned before, the cell size needed to be balanced between the accuracy and reliability for plane detection. The data accuracy (in planarity and vertical direction) and point spacing determined the least cell size. In general, the cell size can be estimated by the tangent value of the vertical accuracy divided by the average of the point spacing. The data accuracy and mean point spacing are generally provided by data vendors. For the Vaihingen dataset, the two values were about 0.1 and 0.5 m, respectively, where,  $\tan \alpha = 0.1/0.5 = 0.2$ , and the angle of  $\alpha$  was about  $12^\circ$ . Hence, the continuous space was quantified by an interval of 0.05, i.e. the histogram had 40, 40, and 20 bins for  $v_x$ ,  $v_y$ , and  $v_z$  components, respectively. For computing convenience, the  $v_x$  and  $v_y$  components were shifted to a non-negative value, and if a component was equal to 1, it was merged into the nearest cell (for the left closed, right open interval  $[0.95, 1)$ , not including 1). When converted to an angle, the distribution of the bins of the histogram was a non-uniform quantization. For example, considering the  $v_x$  and  $v_y$  components only, a variation of 0.05 near the  $0^\circ$  and  $45^\circ$  directions, the angle varied about  $2.9^\circ$  and  $4.2^\circ$ , respectively. Nevertheless, when discretized uniformly in 3D parameter space, no further calculation was needed and the selection of the seed points for planar growing was satisfied. The adjacent distance threshold  $d_{\text{threshold}}$ , which describes the similarity of the normal vectors, was set to 1, i.e. the maximum angle of a local peak in the normal histogram and its 26 neighbours was about  $12^\circ$ .

The co-planarity conditions include an angle and a distance condition, i.e. satisfying the angle threshold and distance threshold. Besides the aforementioned angle threshold  $\alpha$  had a value of about  $12^\circ$ , the distance threshold also was determined by the dataset. In this article, a value of 0.3 m was used, which was about three times the data accuracy and had a tolerance of one and a half of the negative or positive bias.

Another issue pertained to the extracted ‘false’ planes. These spurious planes generally had particular areas and shape factors, namely, small areas (Tables 1–5), and narrow shapes (Figures 6–9). Furthermore, the points near step-edges or parapet walls tend to form inclined planes. Based on this domain knowledge, the false planes were further processed during the reconstruction process. In this article, 3D building models were reconstructed using a proposed new planar patch extraction approach. A 3D building model requires a water-tight roof part (parts); therefore, we attempted to extract planar patches to form an enclosed roof surface, which included some small patches. ‘False’ patches were in fact utilized during the reconstruction process, e.g. a small patch which was adjacent to two parallel patches implied that a step-edge (or step-edge group) existed between the two adjacent planes (Figure 7(g)). A thorough discussion of the reconstruction process was not a part of the scope of this article.

#### 4. Conclusions and future works

Planar patches are the important primitives of polyhedral building models. Prior planar extraction approaches suffered from limitations such as sensitivity to the selection of seed points and/or the lack of computational efficiency. The proposed new planar patch extraction method has the following advantages: (1) it works well on building roof point datasets with arbitrary shapes; (2) it robustly selects the seed points in the reduced dimensional attribute space; (3) the planar patches are segmented within a subset of lidar points (triangles) with similar normal properties when region growing in spatial space; and (4) the entire planar patch extraction process is fully automatic. The experimental results presented in this article confirm that the proposed method can extract various planar patches from simple or complex building point clouds properly and effectively at a high level of quality. The quantitative analysis results indicate that the proposed method is sufficiently robust and the performance improvement is significant.

As planar extraction is limited by the density of the raw lidar points, small roof patches with irregular/regular attachments may result in inaccurate results. A denser point dataset or more knowledge about the roof models could improve the quality of the extraction results and roof patches that are separated by parapet walls may be segmented successfully with the aid of image information. These improvements are planned in the near future.

#### Acknowledgements

The Vaihingen dataset was provided by the German Society for Photogrammetry, Remote Sensing, and Geoinformation (DGPF) (Cramer 2010): <http://www.ifp.uni-stuttgart.de/dgpf/DKEP-Allg.html> (in German).

#### Disclosure statement

No potential conflict of interest was reported by the authors.

## Funding

This work was supported in part by the National Natural Science Foundation of China [Grant Nos 41571434 and 41322010].

## ORCID

Xinyi Liu  <http://orcid.org/0000-0001-5333-8054>

## References

- Awrangjeb, M. 2016. "Using Point Cloud Data to Identify, Trace, and Regularize the Outlines of Buildings." *International Journal of Remote Sensing* 37 (3): 551–579. doi:10.1080/01431161.2015.1131868.
- Awrangjeb, M., and C. Fraser. 2014. "Automatic Segmentation of Raw LIDAR Data for Extraction of Building Roofs." *Remote Sensing* 6 (5): 3716–3751. doi:10.3390/rs6053716.
- Axelsson, P. 1999. "Processing of Laser Scanner Data—Algorithms and Applications." *ISPRS Journal of Photogrammetry and Remote Sensing* 54 (2–3): 138–147. doi:10.1016/S0924-2716(99)00008-8.
- Axelsson, P. 2000. "DEM Generation from Laser Scanner Data Using TIN Adaptive Models." Proceedings of XIX ISPRS Congress, Amsterdam, 110–117.
- Ballard, D. H. 1981. "Generalizing the Hough Transform to Detect Arbitrary Shapes." *Pattern Recognition* 13 (2): 111–122. doi:10.1016/0031-3203(81)90009-1.
- Chen, C., L. Yanyan, L. Wei, and H. Dai. 2013. "A Multiresolution Hierarchical Classification Algorithm for Filtering Airborne Lidar Data." *ISPRS Journal of Photogrammetry and Remote Sensing* 82: 1–9. doi:10.1016/j.isprsjprs.2013.05.001.
- Cramer, M. 2010. "The DGPf Test on Digital Aerial Camera Evaluation – Overview and Test Design." *Photogrammetrie – Fernerkundung – Geoinformation* 2010 (2): 73–82. doi:10.1127/1432-8364/2010/0041.
- De Berg, M., O. Cheong, M. Van Kreveld, and M. Overmars. 2008. *Computational Geometry Algorithms and Applications*. Heidelberg: Springer-Verlag Berlin.
- Duda, R. O., and P. E. Hart. 1972. "Use of the Hough Transformation to Detect Lines and Curves in Pictures." *Communications of the ACM* 15 (1): 11–15. doi:10.1145/361237.361242.
- Edelsbrunner, H., D. Kirkpatrick, and R. Seidel. 1983. "On the Shape of a Set of Points in the Plane." *IEEE Transactions on Information Theory* 29 (4): 551–559. doi:10.1109/TIT.1983.1056714.
- Filin, S., and N. Pfeifer. 2006. "Segmentation of Airborne Laser Scanning Data Using a Slope Adaptive Neighborhood." *ISPRS Journal of Photogrammetry and Remote Sensing* 60 (2): 71–80. doi:10.1016/j.isprsjprs.2005.10.005.
- Fischler, M. A., and R. C. Bolles. 1981. "Random Sample Consensus: A Paradigm for Model Fitting with Applications to Image Analysis and Automated Cartography." *Communications of the ACM* 24 (6): 381–395. doi:10.1145/358669.358692.
- Graham, R. L. 1972. "An Efficient Algorithm for Determining the Convex Hull of a Finite Planar Set." *Information Processing Letters* 1 (4): 132–133. doi:10.1016/0020-0190(72)90045-2.
- Haala, N., and M. Kada. 2010. "An Update on Automatic 3D Building Reconstruction." *ISPRS Journal of Photogrammetry and Remote Sensing* 65 (6): 570–580. doi:10.1016/j.isprsjprs.2010.09.006.
- Jarvis, R. A. 1977. "Computing the Shape Hull of Points in the Plane." Proceedings of IEEE Computer Society Conference on Pattern Recognition and Image Processing, 231–241.
- Kim, C., A. Habib, M. Pyeon, G.-R. Kwon, J. Jung, and J. Heo. 2016. "Segmentation of Planar Surfaces from Laser Scanning Data Using the Magnitude of Normal Position Vector for Adaptive Neighborhoods." *Sensors* 16 (2): 140. doi:10.3390/s16020140.
- Kong, D., L. Xu, and X. Li. 2013. "A New Method for Building Roof Segmentation from Airborne Lidar Point Cloud Data." *Measurement Science and Technology* 24 (9): 095402. doi:10.1088/0957-0233/24/9/095402.

- Kong, D., L. Xu, X. Li, and S. Li. 2014. "K-Plane-Based Classification of Airborne Lidar Data for Accurate Building Roof Measurement." *IEEE Transactions on Instrumentation and Measurement* 63 (5): 1200–1214. doi:10.1109/TIM.2013.2292310.
- Kwak, E., and A. Habib. 2014. "Automatic Representation and Reconstruction of DBM from Lidar Data Using Recursive Minimum Bounding Rectangle." *ISPRS Journal of Photogrammetry and Remote Sensing* 93 (7): 171–191. doi:10.1016/j.isprsjprs.2013.10.003.
- Lari, Z., and A. Habib. 2014. "An Adaptive Approach for the Segmentation and Extraction of Planar and Linear/Cylindrical Features from Laser Scanning Data." *ISPRS Journal of Photogrammetry and Remote Sensing* 93 (7): 192–212. doi:10.1016/j.isprsjprs.2013.12.001.
- Leberl, F., A. Irschara, T. Pock, P. Meixner, M. Gruber, S. Scholz, and A. Wiechert. 2010. "Point Clouds: Lidar versus 3D Vision." *Photogrammetric Engineering & Remote Sensing* 76 (10): 1123–1134. doi:10.14358/PERS.76.10.1123.
- Meidow, J., and H. Hammer. 2016. "Algebraic Reasoning for the Enhancement of Data-Driven Building Reconstructions." *ISPRS Journal of Photogrammetry and Remote Sensing* 114: 179–190. doi:10.1016/j.isprsjprs.2016.02.002.
- Meng, X., L. Wang, J. L. Silván-Cárdenas, and N. Currit. 2009. "A Multi-Directional Ground Filtering Algorithm for Airborne LIDAR." *ISPRS Journal of Photogrammetry and Remote Sensing* 64 (1): 117–124. doi:10.1016/j.isprsjprs.2008.09.001.
- Moreira, A., and M. Y. Santos. 2007. "Concave Hull: A K-Nearest Neighbours Approach for the Computation of the Region Occupied by A Set of Points." GRAPP 2007, Proceedings of the Second International Conference on Computer Graphics Theory and Applications, Barcelona, Spain.
- Nurunnabi, A., D. Belton, and G. West. 2014. "Robust Statistical Approaches for Local Planar Surface Fitting in 3D Laser Scanning Data." *ISPRS Journal of Photogrammetry and Remote Sensing* 96: 106–122. doi:10.1016/j.isprsjprs.2014.07.004.
- Pingel, T. J., K. C. Clarke, and W. A. McBride. 2013. "An Improved Simple Morphological Filter for the Terrain Classification of Airborne LIDAR Data." *ISPRS Journal of Photogrammetry and Remote Sensing* 77: 21–30. doi:10.1016/j.isprsjprs.2012.12.002.
- Qiang, D., and D. Wang. 2004. "Constrained Boundary Recovery for Three Dimensional Delaunay Triangulations." *International Journal for Numerical Methods in Engineering* 61 (9): 1471–1500. doi:10.1002/nme.1120.
- Rabbani, T., F. A. Van Den Heuvel, and G. Vosselman. 2006. "Segmentation of Point Clouds Using Smoothness Constraint." *ISPRS Commission V Symposium 'Image Engineering and Vision Metrology', Dresden*, 248–253.
- Rottensteiner, F., G. Sohn, M. Gerke, J. D. Wegner, U. Breitkopf, and J. Jung. 2014. "Results of the ISPRS Benchmark on Urban Object Detection and 3D Building Reconstruction." *ISPRS Journal of Photogrammetry and Remote Sensing* 93 (7): 256–271. doi:10.1016/j.isprsjprs.2013.10.004.
- Sampath, A., and J. Shan. 2007. "Building Boundary Tracing and Regularization from Airborne Lidar Point Clouds." *Photogrammetric Engineering & Remote Sensing* 73 (7): 805–812. doi:10.14358/PERS.73.7.805.
- Sampath, A., and J. Shan. 2010. "Segmentation and Reconstruction of Polyhedral Building Roofs from Aerial Lidar Point Clouds." *IEEE Transactions on Geoscience and Remote Sensing* 48 (3): 1554–1567. doi:10.1109/TGRS.2009.2030180.
- Shewchuk, J. R. 2002. "Delaunay Refinement Algorithms for Triangular Mesh Generation." *Computational Geometry* 22 (1–3): 21–74. doi:10.1016/S0925-7721(01)00047-5.
- Sun, S., and C. Salvaggio. 2013. "Aerial 3D Building Detection and Modeling from Airborne Lidar Point Clouds." *IEEE Journal of Selected Topics in Applied Earth Observations and Remote Sensing* 6 (3): 1440–1449. doi:10.1109/JSTARS.2013.2251457.
- Sun, S. 2013. "Automatic 3D Building Detection and Modeling from Airborne LiDAR Point Clouds." PhD Thesis, Chester F. Carlson Center for Imaging Science (COS), Rochester Institute of Technology.
- Toth, C., and J. Grzegorz. 2016. "Remote Sensing Platforms and Sensors: A Survey." *ISPRS Journal of Photogrammetry and Remote Sensing* 115: 22–36. doi:10.1016/j.isprsjprs.2015.10.004.

- Verma, V., R. Kumar, and S. Hsu. 2006. "3D Building Detection and Modeling from Aerial LIDAR Data." 2006 IEEE Computer Society Conference on Computer Vision and Pattern Recognition, New York, NY, 2006 June 17, 2213–2220. doi:[10.1109/CVPR.2006.12](https://doi.org/10.1109/CVPR.2006.12).
- Vosselman, G., and B. Gorte. 2004. "Recognising Structure in Laser Scanner Point Clouds." *International Archives of Photogrammetry, Remote Sensing and Spatial Information Sciences* XXXVI - 8/W2: 33–38.
- Vosselman, G., and E. Dijkman. 2001. "3D Building Model Reconstruction from Point Clouds and Ground Plans." *International Archives of Photogrammetry and Remote Sensing* XXXIV-3/W4: 37–43.
- Wang, J., and J. Shan. 2009. "Segmentation of Lidar Point Clouds for Building Extraction." ASPRS 2009 Annual Conference, Baltimore, Maryland, 2009 March 13.
- Xiong, B., M. Jancosek, S. Oude Elberink, and G. Vosselman. 2015. "Flexible Building Primitives for 3D Building Modeling." *ISPRS Journal of Photogrammetry and Remote Sensing* 101: 275–290. doi:[10.1016/j.isprsjprs.2015.01.002](https://doi.org/10.1016/j.isprsjprs.2015.01.002).
- Xu, L., D. Kong, and X. Li. 2014. "On-The-Fly Extraction of Polyhedral Buildings from Airborne Lidar Data." *IEEE Geoscience and Remote Sensing Letters* 11 (11): 1946–1950. doi:[10.1109/LGRS.2014.2314458](https://doi.org/10.1109/LGRS.2014.2314458).
- Zhang, K., J. Yan, and S. C. Chen. 2006. "Automatic Construction of Building Footprints from Airborne LIDAR Data." *IEEE Transactions on Geoscience and Remote Sensing* 44 (9): 2523–2533. doi:[10.1109/TGRS.2006.874137](https://doi.org/10.1109/TGRS.2006.874137).
- Zhang, K., S.-C. Chen, D. Whitman, M.-L. Shyu, J. Yan, and C. Zhang. 2003. "A Progressive Morphological Filter for Removing Nonground Measurements from Airborne LIDAR Data." *IEEE Transactions on Geoscience and Remote Sensing* 41 (4): 872–882. doi:[10.1109/TGRS.2003.810682](https://doi.org/10.1109/TGRS.2003.810682).
- Zhao, Z., Y. Duan, Y. Zhang, and R. Cao. 2016. "Extracting Buildings from and Regularizing Boundaries in Airborne Lidar Data Using Connected Operators." *International Journal of Remote Sensing* 37 (4): 889–912. doi:[10.1080/01431161.2015.1137647](https://doi.org/10.1080/01431161.2015.1137647).
- Zhou, Q.-Y. 2012. "3D urban modeling from city-scale aerial LiDAR data." PhD Thesis, Viterbi School of Engineering, University of Southern California, Los Angeles, California.